Weld Defects in Austenitic Stainless Steel Sheets—Effect of Welding Parameters

Defects grow in number and size as welding current increases, and the type of defect is determined by welding speed

BY V. P. KUJANPÄÄ

ABSTRACT. Two austenitic stainless steel sheets were welded by the autogenous gas tungsten arc process. Defects of different kinds were found to be formed depending on the welding parameters, i. e., cracks, center cavities, cracked center cavities, ripple cavities, undercuts and humps.

The cracks and cavities increased in size and number with increasing welding current, whereas the type of defect was essentially dependent on the welding speed. Center cavities and their cracked versions, as well as undercuts and humps, could occur at high speeds, whereas cracks and ripple cavities were typical of low speeds. The primary austenitic solidification mode augmented cracks and ripple cavities, while the primary ferritic solidification mode increased center cavity formation.

Reasons for the effects of the welding parameters are explored in this paper, together with the occurrence of the different kinds of defects and their formation mechanisms. The practical importance of the results is also discussed.

Introduction

Austenitic stainless steel sheets are extensively used for welded pipes and tubes in the chemical, petroleum and nuclear industries. They are normally assumed to have a good weldability, contrary to steels used for massive constructions that often present problems of solidification cracking and microfissures (Ref. 1-4). The assumption of good weldability is basically true, provided that no high productivity or quality requirements are laid down. However mechanization and automation together with the increasing demand for higher welding speeds have introduced a problem of defect formation in sheet welding.

Defects of different kinds can be created during the welding of austenitic stainless steels, e. g., cracks (Ref. 1-4), pores and cavities (Ref. 5, 6, 7), undercuts and humps (Ref. 8, 9) depending on the welding conditions. These have been encountered using either multiple-electrode gas tungsten arc welding (GTAW) methods, e. g., in pipe production, or single electrode GTAW methods, e. g., in welding pipe bends, flanges or branches (Ref. 10). Many defects may be injurious, especially from a mechanical (Ref. 11-14) or corrosive (Ref. 13) standpoint. Also, they may reduce fatigue (Ref. 14, 15) or creep (Ref. 12) properties.

This paper forms a part of a larger work dealing with the formation of weld defects in GTAW on austenitic stainless steel sheets. The purpose here is to demonstrate the importance of certain welding parameters. Other parts discussing the effects of weld metal composition and shielding gases on the defects are to be submitted for publication at a later date.

Paper presented at the 63th AWS Annual Meeting held in Kansas City, Missouri, during April 25-30, 1982.

V. P. KUJANPÄÄ is a Research Fellow, Laboratory of Physical Metallurgy, University of Oulu, Oulu, Finland.

Table 1—Compositions of the Sheets, wt-%

	Sheet A	Sheet B
C	0.025	0.031
Si	0.49	0.47
Mn	1.54	1.80
P	0.034	0.033
S	0.015	0.017
Cr	17.2	16.9
Ni	12.9	11.2
Mo	2.70	2.66
Cu	0.17	0.18
N	0.030	0.044
Cr_{eq}/Ni_{eq}[(a)]	1.49	1.60

(a) Cr_{eq} = % Cr + 1.37 · % Mo + 1.5 · % Si + 2 · % Nb + 3 · % Ti. Ni_{eq} = % Ni + 0.31 · % Mn + 22 · % C + 14.2 · % N + % Cu. (Ref. 16.)

Experimental Procedures

Materials

Two commercial sheets of AISI Type 316 austenitic stainless steel were used. These were selected so that one (sheet A) would solidify primarily austenitically upon welding and the other (sheet B) primarily ferritically (Ref. 18, 19). The difference was mainly due to differences in the chromium and nickel content, the other elements being at approximately the same level. The compositions are listed in Table 1.

The materials were 2 mm (0.08 in.) thick, and the Ferrite Numbers of the welds varied from 1.3 to 3.1 and from 4.6 to 7.4 in sheets A and B respectively, depending on the welding parameters. The corresponding calculated values are 2.5 and 4.0, based on the DeLong diagram (Ref. 17).

Test Procedure

Mechanized single electrode GTAW methods were used in all the test welds. The welds were produced autogenously on the sheet without a groove.

In the main experiments, 2 × 50 × 250 mm (0.08 × 2 × 10 in.) test sheet was welded to a rigid jig—Fig. 1. Two welds (A and B in Fig. 1) were made in the sheet using the same parameters (i.e., 90 A, 200 mm/min or 7.9 ipm, and 10-12 V) with other conditions as shown in Table 2; this was done in order to equalize the stresses in the sheet before each test.

The test weld proper was made in the middle of the sheet—Fig. 1. The welding parameters were selected on the basis of preliminary experiments in which the test sheets were welded at variable welding speeds and currents in order to determine reasonable values for the main experiments. The other conditions were kept constant and are listed in Table 2.

Figure 2 shows that the weld metal could behave in four different ways, depending on the welding current and speed. If the welding speed was too low compared with the current, the melting was unstable and a hole developed in the sheet; with lower currents or higher speeds, complete penetration or melt-thru occurred. In addition, when the welding speed was too high compared with the current, penetration was incomplete or no fusion occurred—Fig. 2.

Welding currents and speeds for the experiments are depicted in Fig. 2 and in Table 3. Other conditions were kept constant and are indicated in Table 2.

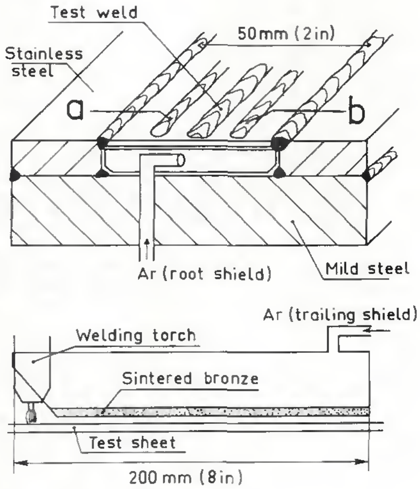

Fig. 1—The test procedure

Table 2—Welding Conditions

Method	Single electrode GTAW
Technique	Mechanized stringer bead
Groove	None
Filler metal	None
Welding position	Flat
Polarity	DC, straight
Welding current	Variable, see Table 3.
Pole voltage	Variable, see Table 3.
Welding speed	Variable, see Table 3.
Arc length	2 mm (0.08 in)
Electrode	EWTh-2, diam 2.4 mm (0.094 in.) and cone angle 60 deg
Arc shielding gas	99.99 % Ar, flow rate—8 L/min (17 cfh)
Root shielding gas	99.99 % Ar, flow rate—8 L/min (17 cfh)
Trail shielding gas	99.99 % Ar, flow rate—8 L/min (17 cfh)
Welding torch	Vertical. Orifice diam—11 mm (0.43 in.); distance from the sheet—10 mm (0.39 in.)

Metallographical Methods

The test welds were pickled in a solution of 15% HNO_3 + 5% HF, and cleaned. They were examined visually, by light stereo microscope and by x-ray radiography (acceleration voltage 90 kV, current 5 mA, exposure time 15-21 min).

The number and length of the defects were measured by the optical stereo microscope on the face and root surfaces of the welds and in the x-ray film. The depth of the defects was determined by the same microscope by focusing separately on the bottom of the defect and the weld surface and then measuring the level difference with a dial gauge. The accuracy of the size measurement was about ± 0.01 mm ($\pm 0.4 \times 10^{-3}$ in.) and the resolution of the film about ± 0.05 mm ($\pm 2.0 \times 10^{-3}$ in.). The shapes and locations of the different kinds of defect were also examined by scanning electron microscope. The microstructure of the welds was also examined by conventional light microscope in the cross section and longitudinal section.

Weld Ferrite Numbers were measured using a Magne-Gage calibrated according to the procedure AWS A 4.2-74.

Results

Defect Classification

Defects of different kinds could be formed depending on the welding parameters. These defects were classified into six types according to shape and macroscopic location in the weld:

1. Cracks.
2. Center cavities.
3. Cracked center cavities.
4. Ripple cavities.
5. Undercuts.
6. Humps.

Their macroscopic locations are indicated in Fig. 3 and their shapes in Fig. 4. The occurrence of defects is seen in Figs. 5-9. The depths of the defects were used as the criteria for the severity of defect formation (except for the ripple cavities where their number was used).

Cracks were situated in the middle region of the weld (Fig. 3A). They were generally 0.5-3 mm (0.02-0.1 in.) long, and longer than the cavities, but were not

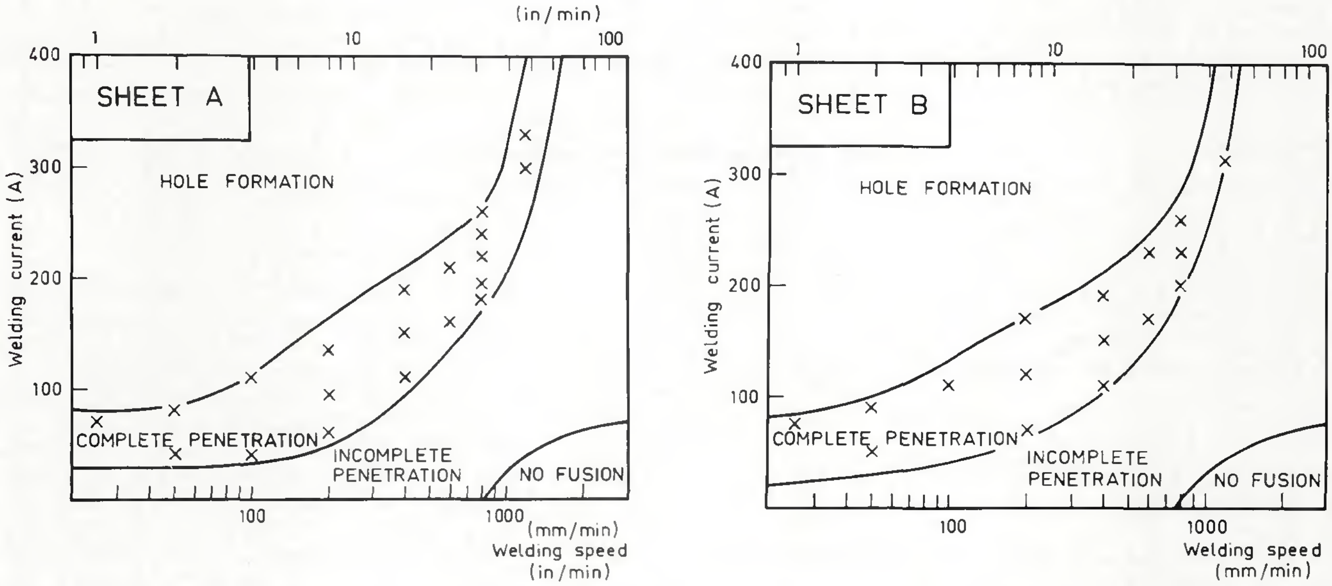

Fig. 2—Fields of penetration in the welding current—welding speed diagram for sheets A and B. The parameters used are marked

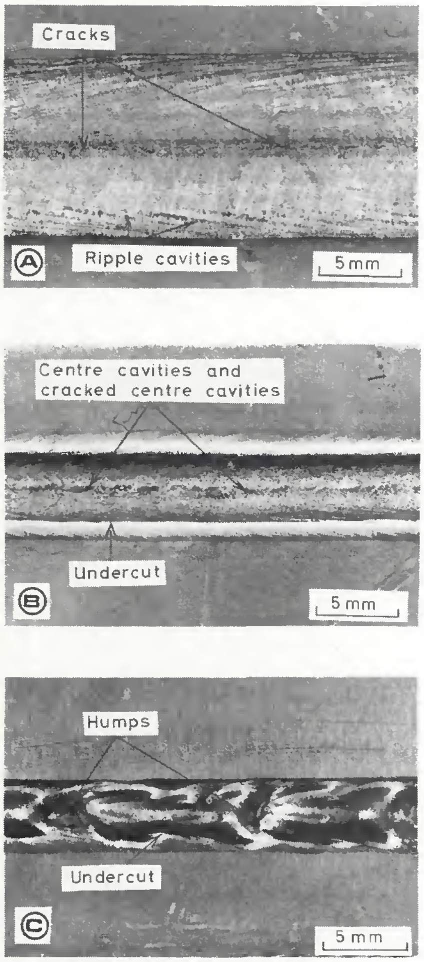

Fig. 3 — Macrographs of welds (sheet A) made using the following parameters: A — 190 A, 14 V, 400 mm/min (16 ipm); B — 330 A, 18 V, 1200 mm/min (47 ipm); C — 180 A, 14 V, 1200 mm/min (47 ipm)

Table 3—Welding Currents, Pole Voltages and Welding Speeds Used in the Main Experiments

	Sheet A		Sheet B	
Welding speed, mm/min (ipm)	Welding current, A	Pole voltage, V	Welding current, A	Pole voltage, V
25 (1.0)	70	10.5	75	10
50 (2.0)	40	10	50	9
	80	11	90	10
100 (3.9)	110	12	110	12
	40	9.5		
200 (7.9)	70	10	70	10
	120	11	120	12
	160	13	170	13.5
400 (15.7)	110	12	110	11.5
	150	13	150	13
	190	14	190	14
600 (23.6)	160	13	170	13
	210	15	230	15
800 (31.5)	180	14		
	195	14	200	14
	220	14.5	230	16
	240	16.5		
	260	16	260	16.5
1 200 (47.2)	300	17	310	18
	330	18		

so numerous (0.01-1.7 per millimeter or 0.25-40 per inch). Their edges were sharp and easily distinguished from the surrounding matrix — Fig. 4A).

The cracks were typically deep (Fig. 5), amounting to 10-25% of the thickness of the weld; they were mostly found in the face surface of the weld. In the microstructure, they were situated in the last regions to solidify, i. e., along the grain boundaries. "Healed cracks"* were also encountered in the microstructure in contact with the cracks proper.

Center cavities were also located in the middle region of the weld — Fig. 3B. They were typically short, 0.03-1 mm (0.001-0.04 in.) in diameter and numerous, 0.4-4 per millimeter (10-100 per inch). They were not very deep, and typically covered 5-15% of the thickness of the weld — Fig. 6. The edges were roundish — Fig. 4B.

Most of the center cavities were open, i. e., they reached the surface. However, some internal cavities or pores were also observed. Center cavities were found approximately to the same extent on the face and root surfaces.

Cracked center cavities (Fig. 3B) were forms comprising a combination of cracks and center cavities. They consisted of low round-edged cavities with cracks in the bottom — Fig. 4C.

The change from crack to center cavity was gradual, and various combinations could be found. These defects were similar in number and size to the uncracked center cavities — Fig. 7.

Ripple cavities were located in rows in ripple lines — Fig. 3A. These were found, in the first place, near the weld interface;

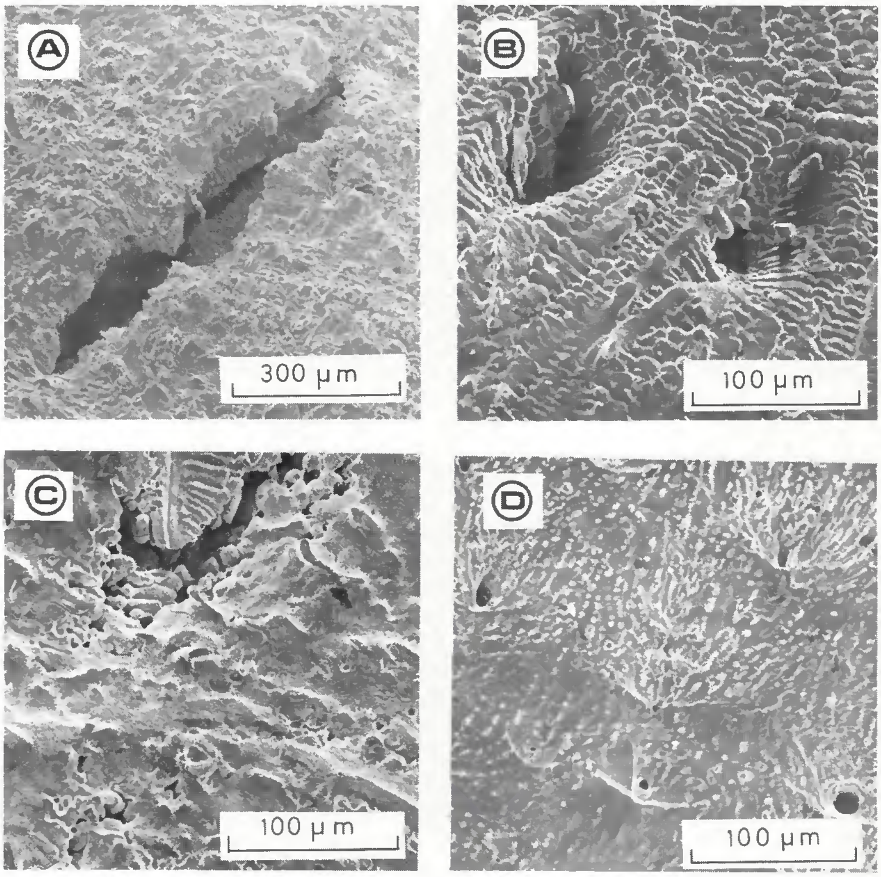

Fig. 4 — Types of defects: A — crack; B — center cavities; C — cracked center cavity; D — ripple cavities

A healed crack is a solidification crack partially or totally backfilled by the melt during solidification (Ref. 21).

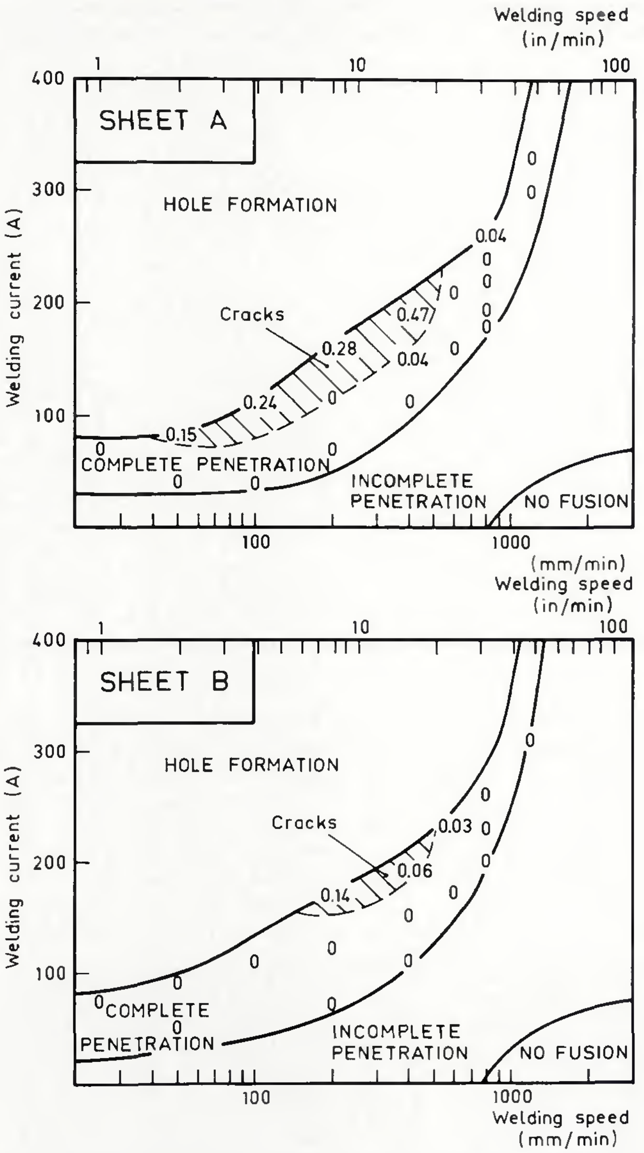

Fig. 5 — Maximum depth of cracks (mm) in the welding current-welding speed diagram. mm/25.4 = in.

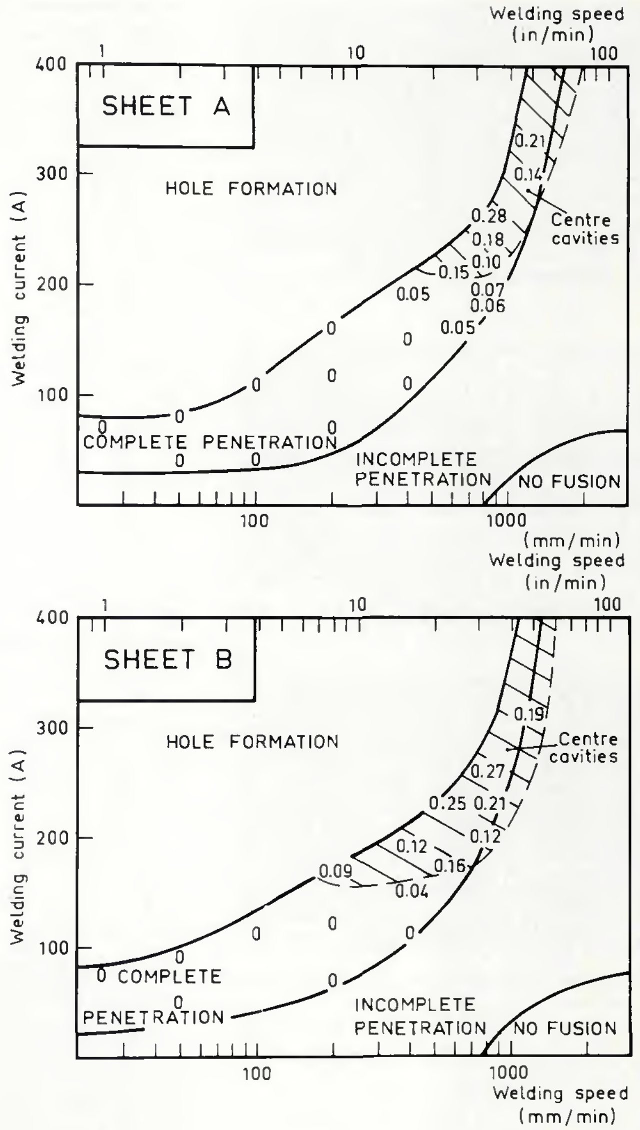

Fig. 6 — Maximum depth of the center cavities (mm) in the welding current-welding speed diagram. mm/25.4 = in.

in the worst cases, they also occurred in the center. They were generally narrow, i. e., 0.02-0.05 mm ($0.8\text{-}2 \times 10^{-3}$ in.) in diameter and not very deep, typically 5-10% of the thickness of the weld.

The ripple cavities were very numerous, as many as 20-30 per millimeter (500-750 per inch) — Fig. 8. Their edges were also roundish — Fig. 4D. The direction of the cavity was parallel to that of solidification. In the microstructure they were found in the last regions to solidify, i. e., along the grain boundaries. These defects were encountered on both the face and the root surfaces of the weld.

Undercuts and humps were large defects. Undercuts were located near the weld interface (Fig. 3B), always forming a continuous groove on both edges of the face surface of the weld. They were generally deep, 10-30% of the thickness of the weld — Fig. 9. The undercuts were well rounded and were always broader than they were deep.

The humps seemed to be associated with a local lack of metal in the middle of the weld and were always surrounded by undercuts — Fig. 3C. Other kinds of defects, such as weld blobs (Ref. 20) or heat-affected zone or crater cracks were also observed, but are not considered here.

Effect of Welding Parameters

The effects of the welding parameters including current and speed on defect formation can best be shown on welding current-welding speed diagrams — Figs. 5-9. The defect fields in Figs. 5-9 are combined in Fig. 10. It can be seen that the weld was most susceptible to crack or cavity formation if the welding parameters were chosen near the hole formation field (Figs. 5-8) when the volume of the weld was high. The lower values of the welding current caused the frequency of defect formation to diminish.

The effect of welding speed was also considerable. Cracks were typically found at low speeds — Fig. 5. When the speed was increased, cracking became pronounced. At medium welding speeds, i. e., ~400 mm/min (15 ipm), the cracks were replaced by center cavities and their cracked versions — Figs. 6, 7 and 10. At even higher speeds, the cavities were further augmented and became mostly pure center cavities.

The formation of ripple cavities was also pronounced at high welding currents — Fig. 8. Unlike the other types of defects, they were favored by a low welding speed, in which case they also existed in the middle region of the weld.

Undercuts were formed only at high welding speeds, i. e., >500 mm/min (>20 ipm) — Fig. 9; also, they were similarly accentuated by high welding currents. Humps were also found at high welding speeds, i. e., >900 mm/min (>35 ipm) — Fig. 9. Characteristically, they were formed only at low welding currents when penetration was incomplete. These results agree well with those for plate welding (Ref. 22).

Effect of Solidification Mode

According to Suutala, et al. (Ref. 18, 19), the solidification mode of the weld can be easily determined on the basis of the microstructure and depends basically on the weld metal composition, i. e., the ratio of chromium and nickel equivalents — Table 1. The materials used in this study — sheets A (Cr_{eq}/Ni_{eq} = 1.49) and B (Cr_{eq}/Ni_{eq} = 1.60) — solidified in the austenitic-ferritic or primary austenitic and ferritic-austenitic or primary ferritic modes, respectively.

The effect of the solidification mode was evaluated comparing the defect fields of sheets A and B on a welding current-welding speed diagram — Fig. 10. It can be seen that the susceptibility to cracking or cavity formation was strongly influenced by the solidification mode. The cracking field was much wider and the cracks much deeper with sheet A, which solidified as primary austenite (Fig. 5), than with sheet B which solidified as primary ferrite; the susceptibility to ripple cavity formation seemed to show the same tendency, although the correlation was not as clear — Fig. 8.

In contrast to crack formation, the center cavities and their cracked versions formed over a much wider welding current-welding speed field in the welds which solidified as primary ferrite than in those which gave primary austenite — Figs. 6, 7 and 10. The depths of these types of defect seemed to be at the same level in both sheets. Undercuts and humps seemed not to be influenced by the solidification mode; the fields in the welding current-welding speed diagram and the depths of the undercuts were approximately the same with both modes.

Reproducibility of Results

The method based on the use of a rigid jig was a suitable and simple test for studying the formation of weld defects under severe conditions. This can be seen from the results of the reproducibility tests, which were performed in three cases — Table 4. For sheet A, cracks and ripple cavities were typically formed under the conditions 110 A and 100 mm/min (4 ipm). As can be seen in Table 4, the reproducibility is good, the standard deviation being only 10–15% of the

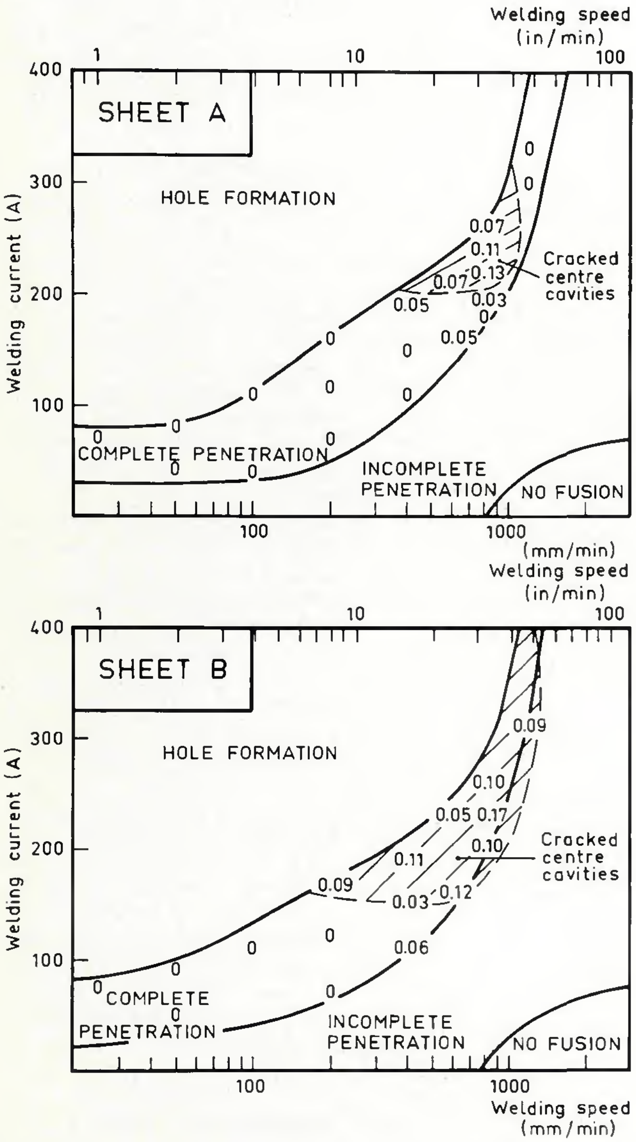

Fig. 7 — Maximum depth of cracked center cavities (mm) in the welding current-welding speed diagram

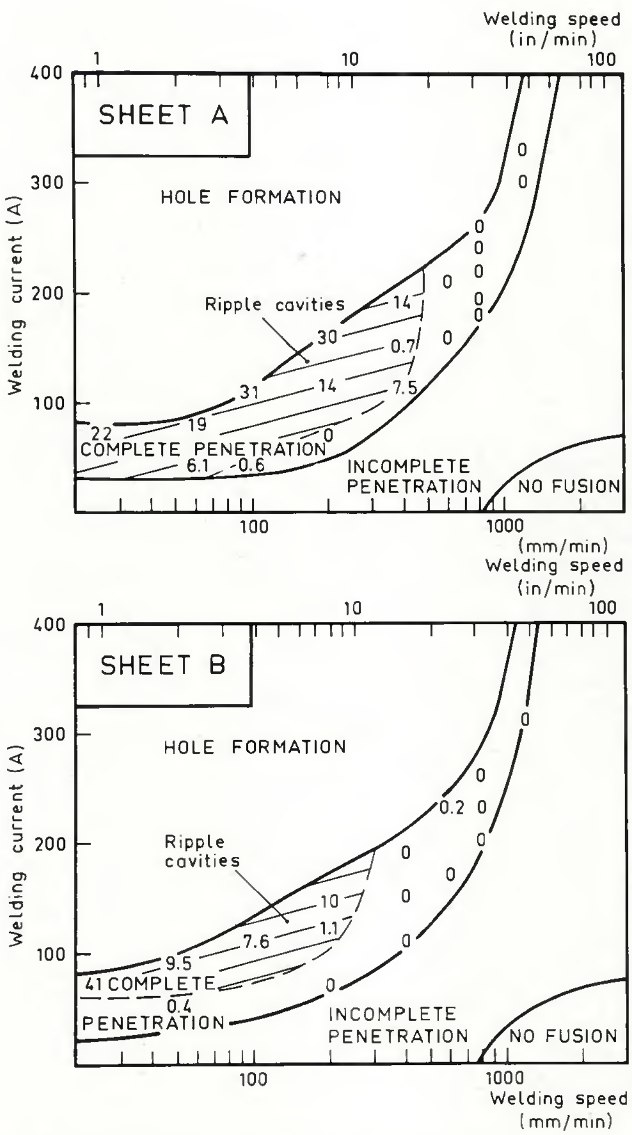

Fig. 8 — Number of ripple cavities (per millimeter) in the welding current-welding speed diagram

Table 4—Reproducibility Results

	Sheet A	Sheet A	Sheet B
Current, A	110	240	260
Speed, mm/min (ipm)	100 (4)	800 (31)	800 (31)
Number of tests	5	5	5
Maximum depth of cracks, mm (in.)			
– Mean value	0.24 (0.010)	–	–
– St. dev.[a]	0.030 (0.0012)	–	–
Maximum depth of center cavities, mm (in.)			
– Mean value	–	0.18 (0.0071)	0.27 (0.011)
– St. dev.[a]	–	0.016 (0.00063)	0.037 (0.0015)
Maximum depth of cracked center cavities, mm (in.)			
– Mean value	–	0.11 (0.0043)	0.10 (0.0039)
– St. dev.[a]	–	0.048 (0.0019)	0.051 (0.0020)
Number of ripple cavities, per millimeter (per inch)			
– Mean value	31 (800)	–	–
– St. dev.[a]	3.6 (91)	–	–
Depth of undercut, mm (in.)			
– Mean value	–	0.13 (0.0051)	0.24 (0.0094)
– St. dev.[a]	–	0.017 (0.00067)	0.030 (0.0012)

[a]Standard deviation using N-1 weighting for example data.

mean values for these defects.

In the other cases tested, sheet A with parameters 240 A and 800 mm/min (31 ipm) and sheet B with parameters 260 A and 800 mm/min, center cavities and their cracked versions and undercuts typically formed. The reproducibility of center cavities and undercuts was also good, the standard deviation being 10–15% of the mean value. However, in the case of the cracked center cavities it was worse, with a standard deviation of about 40–50% of the mean value of the results.

Discussion

Defect Formation Mechanisms

Defect formation mechanisms depend on many variables, among which only the welding parameters are studied here. Thus, it will only be possible to reach definite conclusions on the mechanisms in the later parts of this work after the effects of impurities and shielding gases have also been considered. Some inferences, however, can be made on the basis of the present results.

Cracking in austenitic stainless steels has been widely studied before (Ref. 1–4). It has been found that a weld is prone to solidification cracking if it solidifies with austenite as primary phase and has a normal impurity content (Ref. 4). On the other hand, a weld solidifying as primary ferrite or having a very low phosphorus and sulphur content ($P + S < 0.01$ wt-%) is not susceptible to solidification cracking (Ref. 4, 21).

The cracks found in the sheet welds in this study show the same tendency regarding the solidification mode. In addition, they very much resemble solidification cracks found in thicker plates. Microstructurally, they occurred in the last regions to solidify and were often partially healed or back-filled, evidence that they had been in contact with the melt during solidification. The formation mechanism is thus probably the same as in the case of plates (Ref. 21).

In previous studies on solidification cracking (Ref. 21) the Trans-Varestraint test was used whereby the plate is forced to crack by bending. The present study shows that the cracks caused by the rigidity of the weld, itself, show the same tendency in relation to solidification mode as these forced cracks.

Pores and cavities are traditionally classified into those formed through gas evolution and those formed through shrinkage. Gas pores are usually smooth, rounded, and quite large compared with shrinkage pores which are more irregular in shape.

Center cavities and their cracked versions found in this study had features of both shrinkage and gas pores. Generally, the pure center cavities resembled gas evolution pores more than did the cracked center cavities which tended to have features of shrinkage pores—Figs. 4B and 4C. Matsuda, et al. (Ref. 7) observed these cavities in welds made under an argon atmosphere in a chamber evacuated to 0.13 Pa (10^{-3} mm Hg) before the test. This shows that shrinkage is one reason for the formation of this kind of defect.

The ripple cavities were distinguished from the center cavities on the basis of size, shape and location in the weld. They occurred in the ripple lines and along the grain boundaries, and were parallel to the direction of solidification. Some marks in the microstructure revealed that the space between the grains had probably widened during solidification and had been partially back-filled by the melt, causing a ripple cavity. The ripple cavities were, therefore, in a sense "microscopical cast pipes".

The fact that shrinkage was the main reason for the ripple cavities was supported by the effect of the solidification mode. Segregation is stronger, and the mushy zone is wider when a weld solidifies as primary austenite;. this causes the healing effect to be harder than in primary ferritic solidification, as discussed in connection with cracks.

Undercuts are caused by the melt flow of the weld. The arc pressure forces the melt to flow backwards over the center of the solidifying weld. The melt cools rapidly and its viscosity increases. Thus, it does not have time to become smooth before solidification, and an undercut is formed. The phenomenon may be assisted by the interfacial forces. Humps were probably formed for interfacial reasons, the weld pool being so small that interfacial forces could compel the melt to form these "weld bead turbulents" (Ref. 8, 23).

Defects and Welding Parameters

The volume of the weld pool increased when the welding current was increased; this could have brought about more severe shrinkage and, therefore, larger stresses. In addition, the melt showed a tendency to sink down at high currents and low speeds; this also accentuated the shrinkage during solidification. These were probably the main reasons for the harmful effect of the welding current in promoting crack and cavity formation.

When the welding speed is increased, the form of the weld puddle changes from elliptical to drop-shaped (Ref. 24). With austenitic stainless steel sheets of 2 mm (0.08 in.) thickness, this transition occurs at a speed of about 200 mm/min (8 ipm) (Ref. 19). The content of segregated impurities in the last droplets of the melt was likely greater with drop-formed puddles and, therefore, cracking was also increased—Fig. 5.

The effect of the welding parameters on the undercut can be explained on the basis of the above formation mechanism. When the current was increased, the arc power was greater and forced the melt to flow backwards more easily. The higher welding speed, in turn, made the slope of the weld pool less steep, and it was easier for an undercut to form. At high speeds the melt also had less time to become smooth.

Practical Importance of the Results

The results of this study show that pore-like defects can be reduced, if the

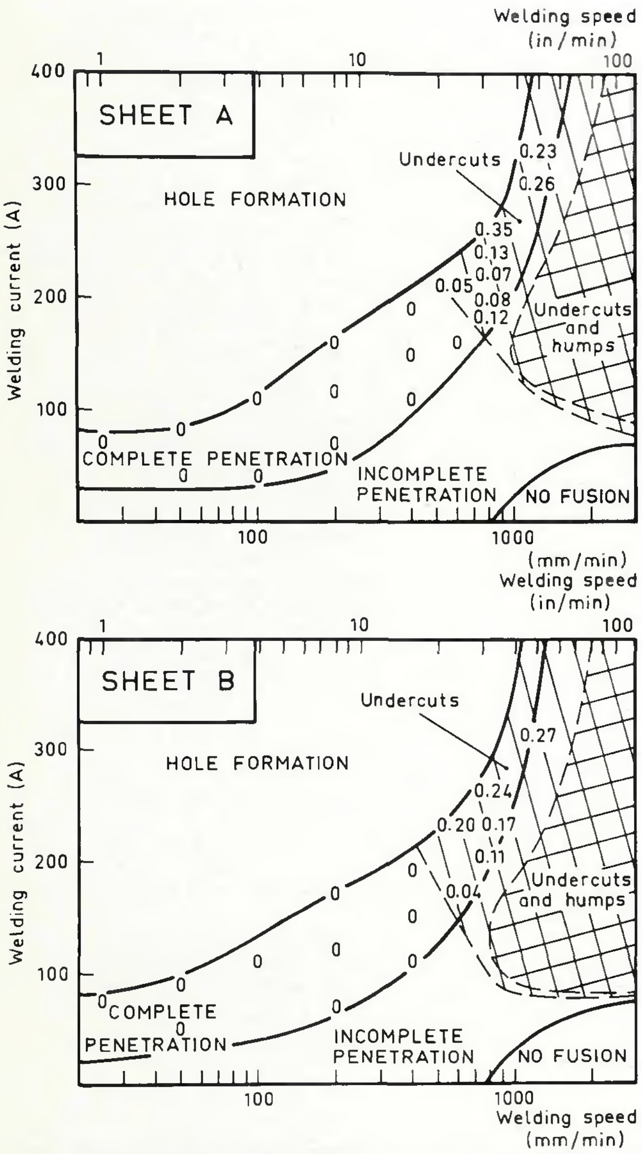

Fig. 9—Depth of undercuts (mm) in the welding current-welding speed diagram. The field of humps is also shown

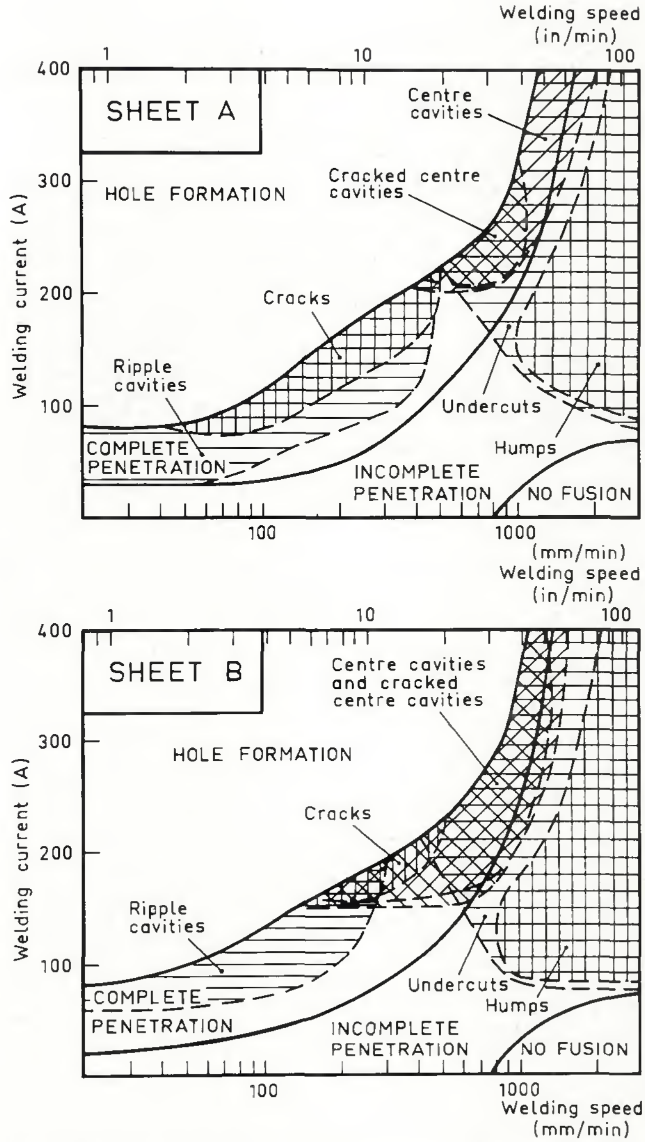

Fig. 10—Fields of various types of defects combined on one welding current-welding speed diagram

welding speed is lowered—Fig. 10. This agrees with the results of Ekerot and Fredriksson (Ref. 25). The present results show, however, that the welding current also has a marked influence on defect formation. Normally, one tries in sheet welding to achieve a defect-free weld with single pass and complete penetration at the maximum welding speed. This study shows that, in a reasonable welding parameter field (i.e., between hole formation and incomplete penetration), the welding current should be kept as low as possible in order to get defect-free welds. In practice, because of the aim for maximum productivity (i.e., high welding speeds), control of the welding current proves to be a very important consideration as seen in Fig. 10.

In this study a rigid test was used wherein the stresses formed were caused by the rigidity of the jig in which the sheet was welded. Thus, it may well serve to describe the welding of a rigid construction. In many cases of sheet welding, however, the rigidity is lower; consequently, the restrictions upon the welding current and speed may be less severe.

The results of this study concern only the single-electrode GTAW process in which the maximum possible welding speed is limited by undercut formation. In multi-electrode GTAW methods, undercuts can be avoided because lower arc pressures are formed on the melt and higher speeds are used (Ref. 9). The formation of center cavities, especially on the root surface, however, may be a problem; it is this that sets one limit upon the use of such methods at the present time.

Conclusions

The defect formation in two austenitic stainless steel sheets with autogenous GTAW was investigated. Particular regard was paid to the shape, size, number and location of the defects and to the effect of the welding parameters. The results allow the following conclusions to be reached:

1. Defects of different kinds can be formed during welding: cracks, center cavities, cracked center cavities, ripple cavities, undercuts and humps.

2. Welding parameters have a marked influence on defect formation. The size and number of the defects increase markedly with the welding current. The welding speed affects the character of the defects. Cracks and ripple cavities are formed at low speeds, while center cavities and their cracked versions and undercuts and humps are typical of high speeds.

3. The solidification mode also exerts an effect on defect formation. Welds

solidifying as primary austenite are more susceptible to crack or ripple cavity formation, while center cavities are more typical of welds solidifying as primary ferrite.

4. Shrinkage is one reason for crack and cavity formation. Undercuts are caused by the effect of arc pressure on the melt flow in the weld.

Acknowledgments

Support from the Foundation of Outokumpu Oy and the Academy of Finland is gratefully acknowledged. The author also thanks Mr. M. Hicks, M. A. for revising the English language of the manuscript.

References

1. Lundin, C. D., DeLong, W. T., and Spond, D. F. 1975. Ferrite-fissuring relationship in austenitic stainless steel weld metals. *Welding Journal* 54(8): 241-s to 246-s.

2. Cieslak, M. J., and Savage, W. F. 1980. Weldability and solidification phenomena of cast stainless steel. *Welding Journal* 59(5): 136-s to 146-s.

3. Gooch, T. G. 1980. Repair welding with austenitic stainless steel MMA electrodes. *Metal Construction* 12(11): 662-631.

4. Kujanpää, V. P., Suutala, N. J., Takalo, T. K., and Moisio, T. J. I. 1980. Solidification cracking—estimation of the susceptibility of austenitic and austenitic-ferritic stainless steel welds. *Metal Construction* 12(6): 282-285.

5. Willgoss, R. A. 1980. Weld pool profile and porosity in the TIG-welding of BS 1501, Type 316, stainless steel. Preprints of an internat. conf.: *Weld pool chemistry and metallurgy*. ed. N. Bailey: 133-145. Cambridge, England: The Welding Institute.

6. Koblyanskii, I. F., and Peshekhonov, V. D. 1967. Porosity in argon arc welding of joints in Kh 18N10T steel sheet. *Welding Production* 14(5): 52-55.

7. Matsuda, F., Hashimoto, T., and Senda, T. 1969. Fundamental investigations on solidification structure in weld metal. *Transactions of national research institute for metals* 11(1): 43-58.

8. Welleans, J. W., and Adams, B. 1969. Undercutting and weld bead turbulence in Tig welding. *Welding and Metal Fabrication* 37(5): 255-257.

9. Anderson, J. E., and Yenni, D. M. 1965. Multi-cathode gas tungsten-arc welding. *Welding Journal* 44(7): 327-s to 331-s.

10. Kujanpää, V. P. 1979. Unpublished research, University of Oulu.

11. Honeycombe, J., and Gooch, T. G. 1973. Effects of microcracks on mechanical properties of austentic stainless-steel weldmetals. *Metal Construction and British Welding Journal* 5(4): 140-147.

12. Harrison, J. D. 1972. Basis for a proposed acceptance—standard for weld defects—Part 1. *Metal Construction and British Welding Journal* 4(3): 99-107.

13. Jubb, J. E. M. 1981. Undercut or toe groove—the Cinderella defect. *Metal Construction* 13(2): 94-98.

14. Petershagen, H. 1981. The effect of undercutting on the fatigue strength of machine-made fillet welds. *Schweissen und Schneiden* 33(4): E54-E56, 165-168.

15. Babaev, A. V. 1980. The effects of pores on the fatique strengths of welded joints. *Automatic Welding* (10): 6-10.

16. Hammar, Ö., and Svensson, U. 1979. Influence of steel composition on segregation and microstructure during solidification of austenitic stainless steels. *Proc. Conf. Solidification and Casting of Metals*. ed. J. Hunt: 401-410. London: The Metals Society.

17. DeLong, W. T. 1974. Ferrite in austenitic stainless steel weld metal. *Welding Journal* 53(7): 273-s to 286-s.

18. Suutala, N., Takalo, T., and Moisio, T. 1979. The relationship between solidification and microstructure in austenitic and austenitic-ferritic stainless steel welds. *Metallurgical Transactions A*. 10A(4): 512-514.

19. Suutala, N. Effect of solidification conditions on the solidification mode in austenitic stainless steels. *Metallurgical Transactions A.*, in press.

20. De Rosa, S., Jacobs, M. H., Jones, D. G., and Sherhod, C. 1979. Studies of TIG weld pool solidification and weld bead microstructures in stainless steel tubes. *Proc. Conf. Solidification and Casting of Metals*. ed. J. Hunt: 416-423, London: The Metals Society.

21. Kujanpää, V., Suutala, N., Takalo, T., and Moisio, T. 1979. Correlation between solidification cracking and microstructure in austenitic and austenitic-ferritic stainless steel welds. *Welding Research International* 9(2): 55-77.

22. Savage, W. F., Nippes, E. F., and Agusa, K. 1979. Effect of arc force on defect formation in GTA welding. *Welding Journal* 58(7): 212-s to 224-s.

23. Bradstreet, B. J. 1968. Effect of surface tension and metal flow on weld bead formation. *Welding Journal* 47(7): 314-s to 322-s.

24. Savage, W. F., Nippes, E. F., and Erickson, J. S. 1976. Solidification mechanisms in fusion welds. *Welding Journal 55* (8): 213-s to 221-s.

25. Ekerot, S., and Fredriksson, H. 1974. Pore formation in the mechanism of stainless steel weld metals. *ESAB-Svetsaren* (1): 8-12.